ADVANCED FUNCTIONAL MATERIALS
www.afm-journal.de

Phase Manipulating toward Molybdenum Disulfide for Optimizing Electromagnetic Wave Absorbing in Gigahertz

Mingqiang Ning, Peiheng Jiang, Wei Ding, Xuebin Zhu, Guoguo Tan, Qikui Man,* Jingbo Li, and Run-Wei Li*

Molybdenum disulfide (MoS_2) has been proved to be a potential electromagnetic wave (EMW) absorber. However, the limited EMW attenuation mechanisms and conductivity have always been recognized as the major challenges impeding their further developments. In this study, a new dielectric tuning strategy giving rise to high EMW attenuation performance by manipulating phase content (with 0, 24, 50, and 100 wt% 1T phase) toward MoS_2 is demonstrated. The greatly introduced 2H/1T interfaces facilitate the dipole distribution dynamics, and the metal-semiconductor mixed phase enhances the electron transfer ability. Benefiting from the structural merits, the MoS_2 with 50 wt% 1T absorber delivers the maximum reflection loss of −45.5 dB and effective absorbing bandwidth of ≈3.89 GHz, corresponding to nearly ten times higher than that of pure 2H counterpart. Moreover, the Computer Simulation Technology (CST) simulation and Lorentz transmission electron microscope are performed to visualize the structural advantages of MoS_2 absorbers with mixed 2H/1T phases. By manipulating the phase compositions, this study provides a deep understanding and opens an avenue in developing efficient and high performance transition metal dichalcogenides (e.g., WS_2, $MoSe_2$, and WSe_2) absorbers.

1. Introduction

As one of electromagnetic response materials, the electromagnetic wave (EMW) absorber has been significantly promoted in EMW technology since the surge of electronics in communication and military applications.[1,2] Thus, the search for EMW absorbers with lightweight, high efficiency, and wide absorption frequency ranges has been always pursued.[2b,c,3] As the widely known 2D transition metal dichalcogenides (TMDs), molybdenum disulfide (MoS_2), which consists of S-Mo-S triple layers, has attracted considerable attentions in electronic and optoelectronic devices owing to their unique electrical and optical properties.[4] In the area of electromagnetic attenuation, the dielectric-dominated EMW absorbing MoS_2 sheet (NMS) absorber was firstly reported in 2015,[5] which exhibited the promising attenuation performance compared to the traditional carbon-based dielectric absorbers. The defect dipole polarization arising from Mo and S vacancies and higher specific surface area of NMS were believed as the main reasons for achieving satisfied EMW consumption. However, it should be noted that the pure TMDs (e.g., MoS_2, WS_2,[6] or VS_2[7]) absorber still suffers from the issues of intrinsic weak electrical conductivity and scanty polarization active sites, which hinders their further application in civil and military electronic devices.[5,8]

To address these issues, significant efforts have been devoted to improving the structural merits of MoS_2 absorbers, including by interfacial constructing, developing novel nanostructures or hierarchical structure design for impedance optimizing. As the fundamental building blocks, MoS_2 combining with various dielectric or magnetic type components for constructing MoS_2-based absorbers (such as MoS_2/rGO,[1b,9] MoS_2@C,[2b] MoS_2/Fe_3O_4,[10] or MoS_2/CNTs[8] etc.) has been regarded as the typical strategy and has shown great potential for ameliorating the EMW absorbing performance. Benefitting from the introduced interfacial polarizations, the MoS_2-based composites present the optimized EMW attenuation ability with respect to its pristine specimen. For instance, the MoS_2/rGO endows the maximum reflection loss (RL_{max}) of −31 dB and the effective attenuation bandwidth (EAB, <−10 dB) of 5.9 GHz as reported by Huang et al.[9a] Liu and co-workers also studied the excellent electromagnetic wave absorption properties of hierarchical flower-like Fe_3O_4/MoS_2 composites with a RL_{max} of −64.0 dB

Dr. M. Q. Ning, Dr. P. H. Jiang, Dr. G. G. Tan, Prof. Q. K. Man, Prof. R.-W. Li
CAS Key Laboratory of Magnetic Materials and Devices
Ningbo Institute of Materials Technology and Engineering
Chinese Academy of Sciences
Ningbo, Zhejiang 315201, China
E-mail: manqk@nimte.ac.cn

Dr. M. Q. Ning, Dr. P. H. Jiang, Dr. G. G. Tan, Prof. Q. K. Man, Prof. R.-W. Li
Zhejiang Province Key Laboratory of Magnetic Materials and Application Technology
Ningbo Institute of Materials Technology and Engineering
Chinese Academy of Sciences
Ningbo, Zhejiang 315201, China

Prof. W. Ding
Institutes of Physical Science and Information Technology
Anhui University
Hefei 230601, China
E-mail: weiding@mail.ustc.edu.cn

Prof. X. B. Zhu
Key Laboratory of Materials Physics
Institute of Solid State Physics
Chinese Academy of Sciences
Hefei 230031, China

Prof. J. B. Li
School of Materials Science and Engineering
Beijing Institute of Technology
Beijing 100081, China

The ORCID identification number(s) for the author(s) of this article can be found under https://doi.org/10.1002/adfm.202011229.

DOI: 10.1002/adfm.202011229

under 1.7 mm.[10b] Our group also reported that the MoS_2@C presented −65 dB attenuation ability under 2 mm and the EAB under −20 dB was ≈3.3 GHz over *K*-band.[2b] In those EMW absorbers as mentioned above, the EMW attenuation performance could be boosted definitely, however, the introduced dielectric or magnetic-type components in composites would hinder the "lightweight" requirements of absorbers in some extent. Therefore, how to prepare the pure MoS_2 absorber with abundant EMW consumption mechanisms still faces huge challenges in obtaining satisfied absorbing performance toward the promising practical application.

Over the past few years, a series of studies have manifested that the phase engineering toward TMDs is an effective strategy for optimizing the electronic structure and has drawn considerate attention in the area of catalysis, energy storage, and biosensing.[4a,11] Compared to the widely existed 2H phase (trigonal prismatic structure), the octahedral coordinated metallic 1T phase demonstrates distinctive physicochemical properties (for example, the faster electron and charge injection/transfer; enlarged interlayer spacing; increased active sites on both basal surfaces and edges, etc.).[11a,e 4c,12] Several studies have provided evidences that the 1T phase has a beneficial effect for achieving better EMW attenuation of TMDs compared to its semiconducting counterpart (2H-MoS_2).[5,9b,13] The recent work reported by Che et al. found that the unique crystalline phase switch between 2H and 1T phase in rose-like 1T@2H-MoS_2/rGO composites was considered to ameliorate the related EMW absorbing performance.[9b] Our previous work also verified that the MoS_2 and WS_2 with moderate content of metallic 1T phase endow the advantages of boosting the EMW absorbing performance over that of pure 2H-MoS_2.[5,13] In view of the superior properties of 1T phase of TMDs, one can expect that the phase manipulating toward MoS_2 (i.e., tuning the 2H/1T phase ratio inside) would be an effective strategy to boost the EMW absorbing performance by the synergistic effect of phase interfaces manipulation and large 2D specific surface area.[11b,14] Nevertheless, three major challenges standing in front of the researchers: i) how to obtain the stable 1T phase regardless of its intrinsic metastable properties; ii) the MoS_2 with 2H and 1T phases should be synthesized in a manner that results in high interface defect density; and iii) the phase ratio should be easily manipulated for the purpose of tuning the dielectric and related EMW attenuation performance.[13,14] Unfortunately, to the best of our knowledge, the research on the relation between the gradually tuned phase composition and the corresponding EMW absorbing performance of TMDs are rarely reported and little has been done to explicitly unravel the underlying EMW attenuation mechanisms involved.

Very recently, our group developed a facile route named magneto–hydrothermal method to prepare MoS_2 with different 2H/1T mass ratio by controlling the external magnetic field (MF) from 0T to 9T.[15] As a result, the unbalanced charge distribution introduced abundant dipoles were introduced across the 2H/1T phase interfaces. Moreover, the as-synthesized MoS_2 possess the high-yield production of 1T phase and are ambient-stable for more than one year. Therefore, this newly developed strategy provides the possibilities of correlating the EMW absorbing properties with the detailed phase composition of MoS_2.

Herein, we prepared the MoS_2 absorbers with mixed semiconductive 2H and metallic 1T phase compositions under different mass ratio, resulting in the introduction of abundant phase interfaces and optimizing of conductivity. As such, the EMW absorbing properties were continuously tuned under different 2H/1T mass ratio. The MoS_2 with 50 wt% 2H and 50 wt% 1T phase (embedded each other) exhibited the optimal EMW absorbing performance with an RL_{max} of −45.5 dB, which was nearly ten times as high as that of pure 2H counterpart. By the characterization of scanning transmission electron microscopy (STEM), Lorenze transmission electron microscope (TEM) and Computer Simulation Technology (CST) simulations, the significantly optimized EMW absorbing performance of MoS_2 was attributed to the strong charge transfer at the 2H/1T phase interfaces and moderate optimized conductive loss. This work represents the first attempt to bring an effective phase composition tuning to MoS_2 for the demonstration of its effectiveness in EMW attenuation determining and versatility toward TMDs.

2. Results and Discussion

The MoS_2 sheet with pure or mixed phase were synthesized via the magneto-hydrothermal strategy as illustrated in **Figure 1**. The 1T-MoS_2 displays a net magnetic moment on Mo atoms compared to the diamagnetism of 2H-MoS_2 according to the density functional theory calculation results.[16] Meanwhile, as a type of important thermodynamic parameters in materials processing, the MF could transfer high energy on an atomic scale of substances, resulting in the expected atomic and molecular

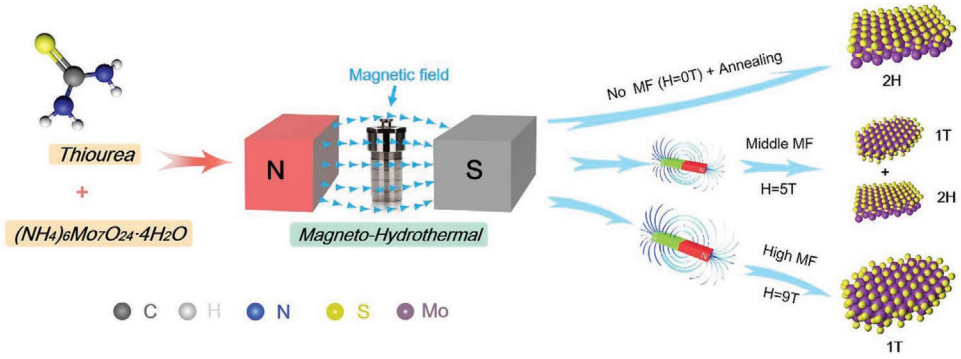

Figure 1. Schematic illustration of the synthesis route of MoS_2 with pure or mixed phases.

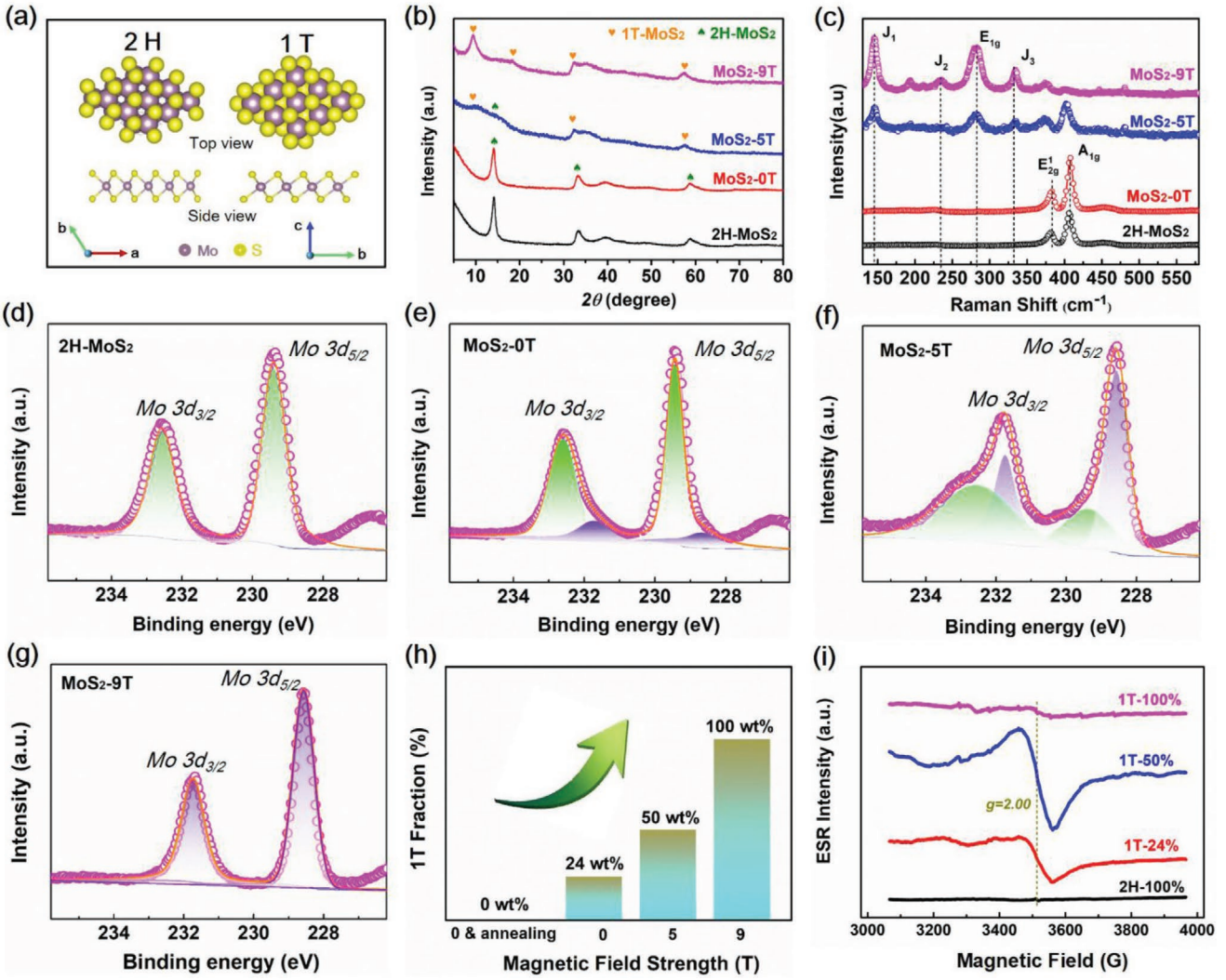

Figure 2. a) Schematic of atomic structure for 2H- and 1T-MoS_2; b) XRD patterns, c) Raman spectra; high-resolution XPS spectra from the Mo 3d region of d) 2H-MoS_2, e) MoS_2-0T, f) MoS_2-5T and g) MoS_2-9T; h) 1T phase percentage, and i) EPR spectra of mixed phase of MoS_2.

alignments.[15,17] During the magneto-hydrothermal treatment, with the introduction of magnetic fields, an extra magnetic free energy ($E_M = -\mu_0 \chi V H^2/2$; μ_0 is the permeability of vacuum, V is the volume, and H is the magnetic field strength) will be induced. Considering the different volumetric magnetic susceptibility (χ) values of two phase ($\chi_{1T} > \chi_{2H}$), the pure 1T phase were gradually formed under a higher MF condition.[15]

Figure 2a displays the schematic of two atomic structure of obtained MoS_2: the thermodynamically stable 2H (trigonal prismatic) and the metastable 1T phase (octahedral). For the trigonal 2H phase, each molybdenum atom is prismatically coordinated by six surrounding sulfur (S) atoms and the S atoms in upper layers are located directly above those on the lower layers.[4a,b] As a contrast, the S atoms in the upper and lower planes are offset from each other and the Mo atoms occupy the octahedral holes of the S layers for the octahedral 1T phase.[4b,11a,12] Figure 2b shows the powder X-ray diffraction (XRD) patterns of four MoS_2 absorbers obtained under different MF conditions (0T & annealing, 0T, 5T, and 9T). All characteristic peaks of absorbers match well with the standard JCPDS card (PDF#: 87–2416) of MoS_2. However, the (002) lattice plane (normally 2θ = 14.34°, corresponding to the interplanar spacing of 6.15 Å) gradually shifts to a lower diffraction angle as the MF changing from 0T to 9T, indicating the increased mass content of 1T phase and the expansion of interlayer distance (increased to 9.4 Å, discussed below).[4c,15] Raman and X-ray photoelectron spectroscopy (XPS) spectra analyses were employed to investigate the mixed phase characteristics of four absorbers. As presented in Figure 2c, two typical Raman peaks at ≈378 and 404 cm^{-1} are evident from the E_{2g}^1 (in-plane displacement and shear force between Mo and S atoms) and A_{1g} (symmetric displacement and compressive force between S atoms along *c*-axis) modes, confirming the 2H crystal structure in 2H-MoS_2 and MoS_2-0T.[1b,4c] As a contrast, the additional peaks centered at 146 (J1), 234 (J2), and 335 (J3) cm^{-1} can be clearly observed for MoS_2-5T and MoS_2-9T absorbers, which are considered as the 1T phase signal according to the previous studies.[11b,18] The gradually increased intensity of J1, J2, and J3

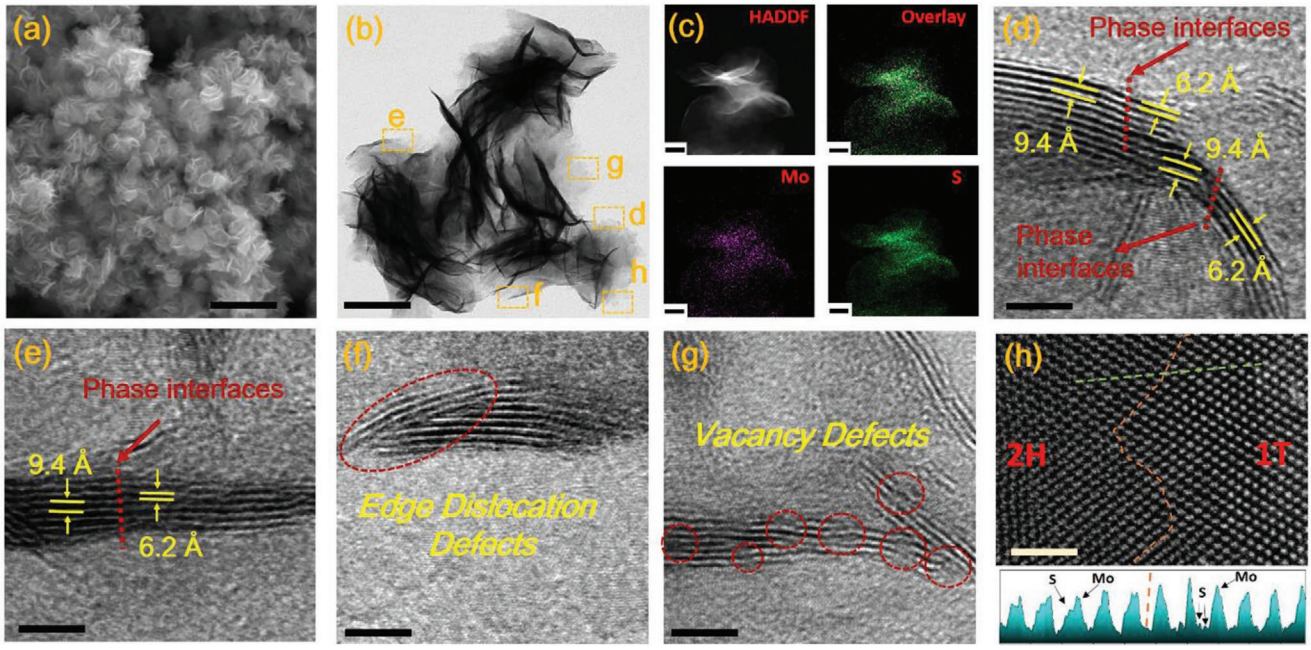

Figure 3. a) SEM, b) TEM, c) HADDF-STEM mappings, d–g) HRTEM, and h) STEM images of 1T-50% absorbers; Insets in (h) is the intensity profile along the olive green line; Scale bar in (a), (b), (c), (d-g), and (h) are 500, 100, 50, 5, and 2 nm, respectively.

peaks indicates the growing 1T content in MoS_2-5T and MoS_2-9T absorbers. Moreover, by deconvoluting the Mo 3d regions of four MoS_2 absorbers (Figure 2d–g), the 1T phase mass percentage under 0, 5, and 9 T increased almost linearly and were estimated to be ≈24, ≈50 and ≈100%, respectively. As a result, the above four absorbers were denoted as 2H-100%, 1T-24%, 1T-50%, and 1T-100% accordingly. Clearly, the percentage of metallic 1T phase in MoS_2 present the gradual upward trend as the increasing of magnetic field from 0T to 9T (Figure 2h). According to the study,[19] the electronic properties of TMDs are closely related to its structural properties and the electronic conductivity of 1T-MoS_2 is superior to the semiconducting 2H counterpart (≈10^7 fold). Figure S1, Supporting Information, shows the conductivity of MoS_2 as a function of 1T phase content of 30 wt% MoS_2/wax. It is found that the conductivity of MoS_2 increases slowly as 1T content are less than 24 wt%, however, reaches to 1.23×10^{-3} and 5.06×10^{-3} S m^{-1} as 1T content are 50 and 100 wt%, respectively. Apparently, the conductivity behavior of MoS_2 are consistent with that of 1T phase content as shown in Figure 2h, verifying the beneficial metallic characteristics of 1T phase. The phase-manipulated electrical conductivity may endow MoS_2 with adjustable conduction loss, thus achieving the satisfied EMW stealth performance. In addition, the electron paramagnetic resonance (EPR) spectra were also performed to provide more insight into the existence of atomic vacancies of four absorbers. As shown in Figure 2i, compared to the weak EPR signal (at g = 2.00) of pure phase absorbers (2H-100% and 1T-100%), the intensified and broadened resonances were observed for 1T-24% and 1T-50% absorbers, indicating the increased concentration of sulfur vacancy in those absorbers with mixed phase.[16c]

To further examine the morphologies and structures of four absorbers, scanning electron microscopy (SEM) and transmission electron microscopy (TEM) measurements were employed. The SEM and TEM images (**Figure 3**a,b and Figure S2, Supporting Information) show the typical rippled morphologies with size of around 200 nm, indicating the flexible and ultrathin nature of the as-synthesized MoS_2 absorbers.[4a,b,20] The high-angle annular dark-field scanning transmission electron microscopy (HAADF–STEM) image and element distribution maps were conducted to verify the obtaining of MoS_2 (Figure 3c) and the applied magnetic field (from 0T to 9T) has no effect on the intercrossed curved nanosheets structures of MoS_2 samples. To closely examine the nanostructures of MoS_2 absorbers, take 1T-50 wt% as the example, the high resolution TEM (HRTEM) images were conducted. As shown in Figure 3d–g (taken from the specific magnified TEM image in Figure 3b), compared to the 6.2 Å interplanar spacing of 2H phase, the obvious enlarged lattice fringes with a distance of 9.4 Å can be attributed to the expanded (002) plan of 1T phase, which were introduced during the magneto-hydrothermal process.[15,21] The HRTEM results are consistent with the XRD results (Figure 2b). In addition, two different interplanar spacing (9.4 and 6.2 Å) in the nearby area were also observed as marked by the red arrows in Figure 3d,e, verifying the coexistence of 2H and 1T phases within a single MoS_2 sheet. To offer more insights into the mixed phase structures of MoS_2, the HAADF-STEM image were carefully examined and the coexistence of mixed phases within the individual MoS_2 sheet were found as shown in Figure 3h. The intensity profile across the phase interface also confirms the coherently distributed mixed phases in a single MoS_2 sheet. On the basis of this structural merit and different work function for 2H (5.86 eV) and 1T (5.26 eV) phase, the electrons tend to transfer from 1T phase to 2H phase across the metal-semiconductor phase interfaces (i.e., the 2H/1T interface), thereby exhibiting

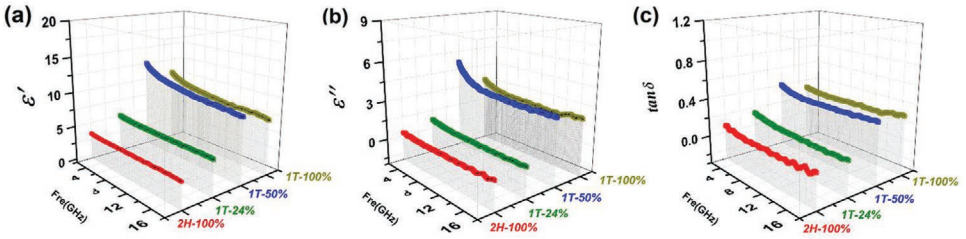

Figure 4. a) ε'-f, b) ε''-f, and c) $tan\delta E$-f curves of 2H-100%, 1T-24%, 1T-50%, and 1T-100% absorbers under 50 wt% mass loadings.

super dipole distribution dynamics.[16c,22] The distribution of charge density difference calculated by first-principles density functional theory also confirms the obvious electric dipoles over 2H/1T interfaces of MoS_2 (Figure S3, Supporting Information). In addition, the displacement of atoms around the interfaces also results in the enhancement of electron transfer ability, thus providing the optimized conductive loss toward the EMW attenuation. Moreover, consistent with the EPR results as shown in Figure 2i, the lattice distortions (such as edge dislocation and point defect as shown in Figure 3f,g) were also manifested under the strong external MF. According to the classic dielectric loss theory,[2a,b,8] the affluent vacancies are also beneficial to the forming of dipoles, thus endowing the potential of consuming EMW efficiently.

In general, the complex permittivity ($\varepsilon_r = \varepsilon'-i\varepsilon''$) and complex permeability ($\mu_r = \mu'-i\mu''$) are the two key electromagnetic parameters for determining the microwave absorbing performance of EMW absorbers.[3a,23] The ε' and μ' represent the storage capability of EMW, while the ε'' and μ'' reflect the attenuation ability of EMW, respectively. Due to the nonmagnetic characteristics of TMDs, the ε_r were measured ≈1.0 and ≈0 as shown in Figure S4, Supporting Information, thereby suggesting a negligible magnetic loss in MoS_2 absorbers.

Figure 4a–c display the ε_r-f curves of 2H-100%, 1T-24%, 1T-50%, and 1T-100% MoS_2 absorbers, together with the calculated $tan\delta_E$-f curves (Figure S5, Supporting Information). With the increase in frequency to 18 GHz, the ε_r values presented the decreasing trend, which could be attributed to the lags induced in the absorbers to follow the reversing EMW in a higher frequency.[2b,24] The ε', ε'' and $tan\delta_E$ values of four absorber present the upward trend under the 40, 50, and 60 wt% mass loading, which could be well explained by the effect medium theory.[5,9b] However, it is noteworthy that the MoS_2 absorbers with different 1T phase content display the different dielectric behaviors under the given mass loadings, i.e., the 50 wt% mass loading absorber displays the ε' and ε'' values in the order of 1T-50% > 1T-100% > 1T-24% > 2H-100%, while 1T-100% >1T-50%> 1T-24%> 2H-100% under the 40 and 60 wt% mass loadings. Considering the boosted interfacial and dipole polarizations (the existence of abundant 2H/1T phase interfaces as evidenced by HRTEM, XPS results and the following Lorentz-off-axis electron holograms; the defects confirmed by the HRTEM and EPR) in 1T-50% absorber, it is reasonable to speculate that the strong polarization should play the dominate roles in obtaining the enhanced ε' and ε'' values. As a contrast, the dielectric polarizations may be hidden by the conductivity loss when the mass loading is 40 wt% (the weaker polarization ability) or 60 wt% (the easier forming conductive network).[25] The Cole–Cole plots also verify the existence of Debye relaxation processes in absorbers as marked by small circles (Figure S6, Supporting Information), especially in the 1T-50% absorber.[23,26] In addition, to verify the boosted EMW attenuation advantages of 1T-50% MoS_2 absorber (with sufficient 2H/1T phase interfaces), the absorber mixed by 50wt% 2H-100% absorber, and 50wt% 1T-100% absorber (denoted as 1T(50%)/2H(50%)-MoS_2) was also examined. As shown in Figure S7, Supporting Information, though displaying the similar magnetic characteristic (Figure S7d, Supporting Information), the 1T-50% absorber still shows the obvious enhanced permittivity and $tan\delta_E$ values (Figure S7a–c, Supporting Information) over the frequency range compared to 1T(50%)/2H(50%)-MoS_2 absorbers. In addition, as mentioned above, the 2H/1T phase interfaces were prone to form under the MF, thus exhibiting interfacial polarization advantages over the physically mixed one (Figure S7e, Supporting Information).

To evaluate the EMW absorbing performance of MoS_2 absorbers with different phase, the RL values of four absorbers were calculated according to the transmission line theory as described in Electromagnetic Measurements Part. Figure S8, Supporting Information, shows the RL-f curves of 2H-100%, 1T-24%, 1T-50%, and 1T-100% absorbers with 40, 50, and 60 wt% mass loadings under 1.6–4.8 mm. Note that the absorbers with 50 wt% mass loading exhibited the optimal EMW absorbing performance over 2–18 GHz, the 2D and 3D RLs-f plots of 2H-100%, 1T-24%, 1T-50%, and 1T-100% absorbers under the same thickness range and mass loading were further plotted and compared.

As shown in **Figure 5**a,b, the RL_{max} of 2H-100% and 1T-24% absorbers are merely −2.8 dB (2.8 mm) and −3.8 dB (4.8 mm), respectively. The 2D RLs-f plots also clearly display that there are no effective EMW absorbing areas (<−10 dB), indicating the limited EMW absorbing ability of 2H-phase dominated MoS_2 absorbers. With the increasing 1T phase content in MoS_2, the RL_{max} and EAB values of 1T-50% absorber dramatically decreases to −45.5 dB (3.5 mm) and ≈3.89 GHz (2 mm) (Figure 5c), showing the obviously optimized EMW attenuation performance compared to 2H-100%, 1T-24%, and 1T(50%)/2H(50%) MoS_2 absorbers (Figure S7f, Supporting Information). However, it should be pointed out that further increased 1T content in MoS_2 will lead to the deterioration of related performance: the 1T-100% absorber just endows an RL_{max} of −17 dB (4.0 mm) and an EAB of ≈3.2 GHz (2 mm) as shown in Figure 5d. According to previous studies,[1b,8] the improper conductivity could lead to the weak entrance of incident EMW (i.e., poor impedance matching, discussed below). Considering the monolithic 1T phase in 1T-100% absorber, it is

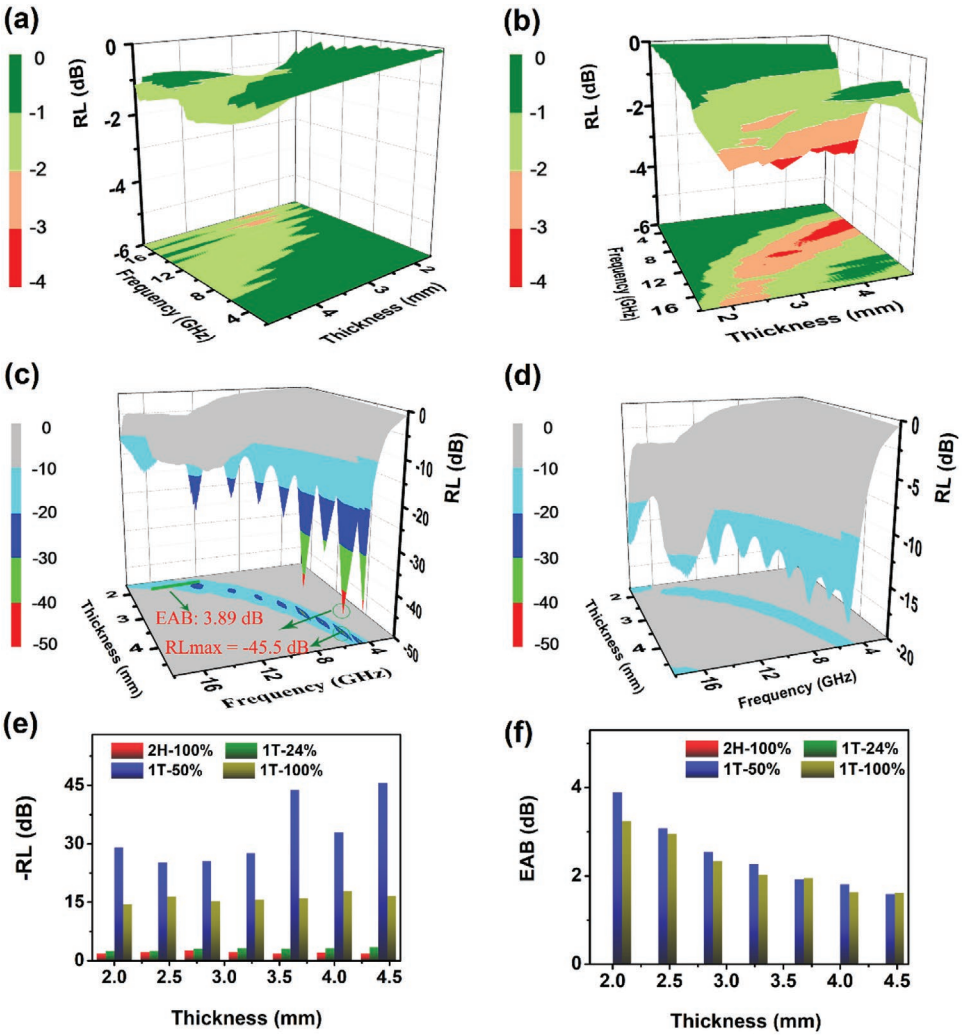

Figure 5. 3D *RLs-f* curves and 2D projection plots of a) 2H-100%, b) 1T-24%, c) 1T-50%, and d) 1T-100% absorbers with 50 wt% mass loadings under 1.6–4.8 mm; e) and f) are the RL and EAB comparison curves of absorbers under the same thicknesses.

supposed that the huge enhanced conductivity should respond for its poor absorbing performance.

Based on above results, it can be concluded that there is an interdependent relationship between 1T phase content and the EMW absorbing performance of MoS_2. As compared and shown in Figure 5e,f, the stealth performance (RLs and EAB values) of MoS_2 can be manipulated by the phase engineering. Specifically, the 1T-50% MoS_2 absorber renders the strongest absorption with an RL value of –45.5 dB under ≈3.5 mm with an EAB of 2 GHz and the 2H/1T phase interfaces existed in the absorbers should be responsible for the corresponding amelioration. Meanwhile, the 1T-50% absorber also presents the satisfied attenuation performance under a thinner thickness (2–3.2 mm) with the wider EAB values (2–4 GHz) as shown in Figure 5f.

Generally, the attenuation constant (α) and impedance match degree (Δ) are the two crucial factors for evaluating EMW absorbers. To understand the underlying phase-dependent EMW attenuation mechanisms of MoS_2 absorbers, the α and Δ were systematically studied. Figure S9, Supporting Information, shows the α-*f* values of four MoS_2 absorbers with different mass ratio of 1T phase. Consistent with the ε''-*f* and $tan\delta_E$-*f* curves as presented in Figure 4 and Figure S5, Supporting Information, the 1T-50% absorber also reasonably delivers the highest α values compared to other three absorbers over the investigated frequencies, providing the premise for achieving high performance EMW absorbers. The abundant 2H/1T interfaces and moderate conductivity in 1T-50% absorber should responsible for the boosted α values.

Figure 6a–d compares the Δ-*f* values of four MoS_2 absorbers with 50 wt% mass loading under 1.6–4.8 mm. According to previous studies,[2a,26] the Δ of absorbers close to zero ($|\Delta| < 0.4$, close to free space) implies the obtaining of satisfied impedance matching values. As observed, the 1T-50% and 1T-100% absorber have a wide small Δ values (0–1.2) over 2–18 GHz, indicating the good impedance matching characteristics (Figure 6c,d). As a contrast, the 2H-100% and 1T-24% absorbers display the larger Δ values (2.0–4.0) (Figure 6a,b). However, it is worthy of note that the 1T-24% and 2H-100% absorber still possess the impedance matching advantage at high frequencies as reported in other various absorbers.[2a,10a] Combined with above

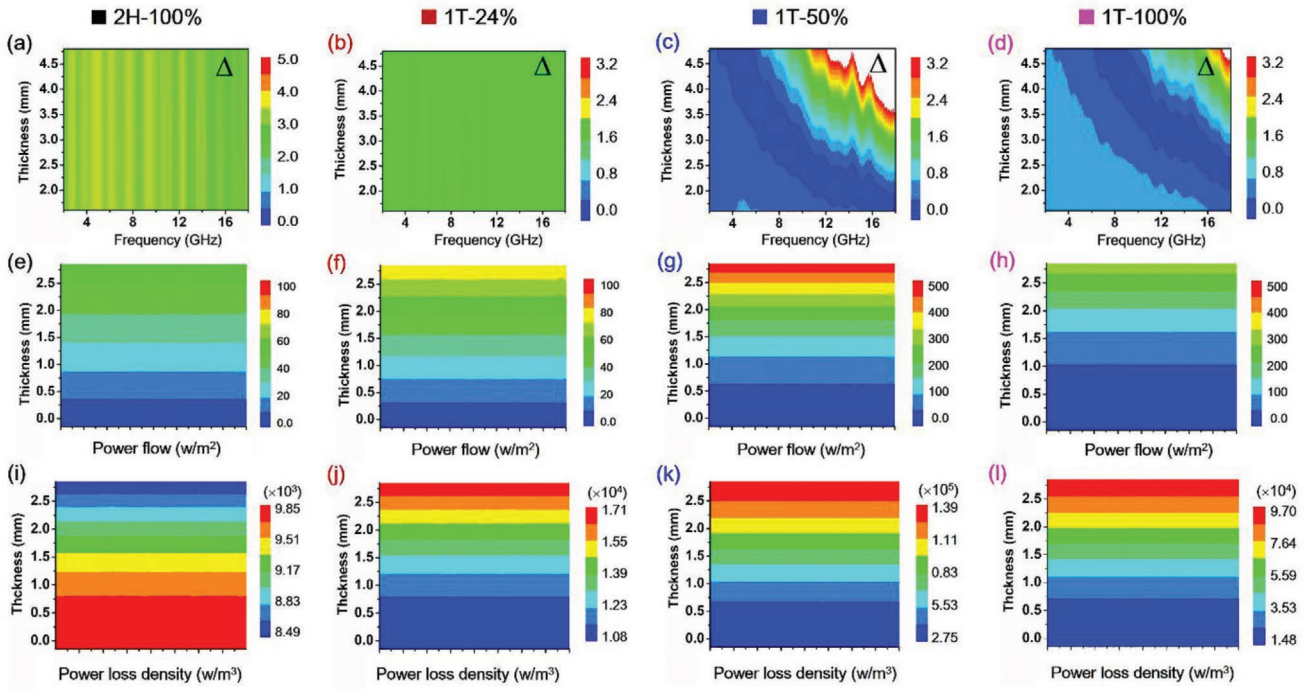

Figure 6. a–d)Δ-*f* maps (1.6–4.8 mm), CST simulated e–h) power flow, and i–l) power loss density (3 mm @ 6 GHz) of (a,e,i) 2H-100%, (b,f,j) 1T-24%, (c,g,k) 1T-50%, and (d,h,l) 1T-100% absorbers with 50 wt% mass loading with wax.

α-*f* results of four absorbers, it is easy to find that the enhanced *α* values and optimized Δ performance together determine the excellent EMW absorbing performance of 1T-50% absorber.

To intuitively illustrate the movement and attenuation processes of EMW inside of absorbers, the power flow (W m^{-2}) and power loss density (W m^{-3}) of incident EMW toward MoS_2 absorbers were carried out by CST simulations. Figure 6e–h shows the power flow density of 2H-100%, 1T-24%, 1T-50%, and 1T-100% MoS_2 absorbers with 50 wt% mass loading under 3 mm at 6 GHz. As clearly seen, the power flow entering absorbers presents the trend in the order of 1T-50% > 1T-100% > 1T-20% > 2H-100%, verifying the impedance characteristics of four absorbers as demonstrated in Figure 6a–d. Figure 6i–l presents the power loss density of four absorbers. The gradual decreasing values of power loss density confirms the gradual EMW consuming inside absorbers and the four MoS_2 absorber also exhibit the attenuation capacity in the order of 1T-50% > 1T-100% > 1T-20% > 2H-100%. Obviously, the CST simulation results reveals that the 1T-50% should endow the optimal EMW consumption ability, which are well consistent with the *RL*-*f* curves as displayed in Figure 5a–d. The CST simulation results confirm the hypothesis that the EMW absorbing performance of MoS_2 can be tuned by manipulating the 1T phase ratio.

To further clarify the fact that the abundant 2H/1T interfaces and atomic defect of 1T-50% leading to the enhanced Debye polarization behaviors as mentioned above, the Lorentz off-axis electron holograms were performed based on the holography method.[27] According to the reported literatures,[24,27] although the charge density generated by interfacial polarizations cannot be obtained quantitatively, the obviously charge heterogeneity can be still qualitatively verified by the off-axis electron holograms. As **Figure 7**a–l shows, four absorbers display the different charge density on the ultrathin specimen as marked by the dashed orange line. By comparing with those blank situations (Figure S10, Supporting Information), the absorbers with mixed phases, especially for 1T-50%, demonstrate the obvious electron distribution information (i.e., the charge unbalance), indicating the abundant phase interfaces/atomic defects inside. Therefore, when applied as the EMW absorber under the external electromagnetic field, the abundant 2H/1T interfaces/defects in 1T-50% absorber could take effect as polarizations center for attenuating incident EMW, thus presenting the optimal EMW absorbing performance.

On the basis of above results, the possible phase-manipulated EMW attenuation mechanisms of MoS_2 were proposed as schematically illustrated in **Figure 8**. The 2H/1T phase interfacial polarization, dipole orientation polarization caused by the vacancy defects and the conductance loss were the main loss mechanisms in MoS_2 with mixed phases. In details: 1) owing to the large number of introduced phase interfaces between 2H and 1T, abundant interfacial polarizations over the investigated frequencies can be achieved, leading to the increased active sites for Maxwell–Wagner–Sillars interfacial polarizations compared to the pure 2H or 1T phase MoS_2. Moreover, the interfacial polarizations ability varies with the exact 1T phase content in the MoS_2, and endows the strongest values as the 1T content is 50 wt% (Figure 8a,b–i); 2) the external MF during the synthesis process could lead to the formation of point defects such as sulfur vacancies. The uneven distribution of local charges results in the formation of dipole orientation polarization, which displays the similar dielectric behavior as that of interfacial polarization (Figure 8a,b-ii).

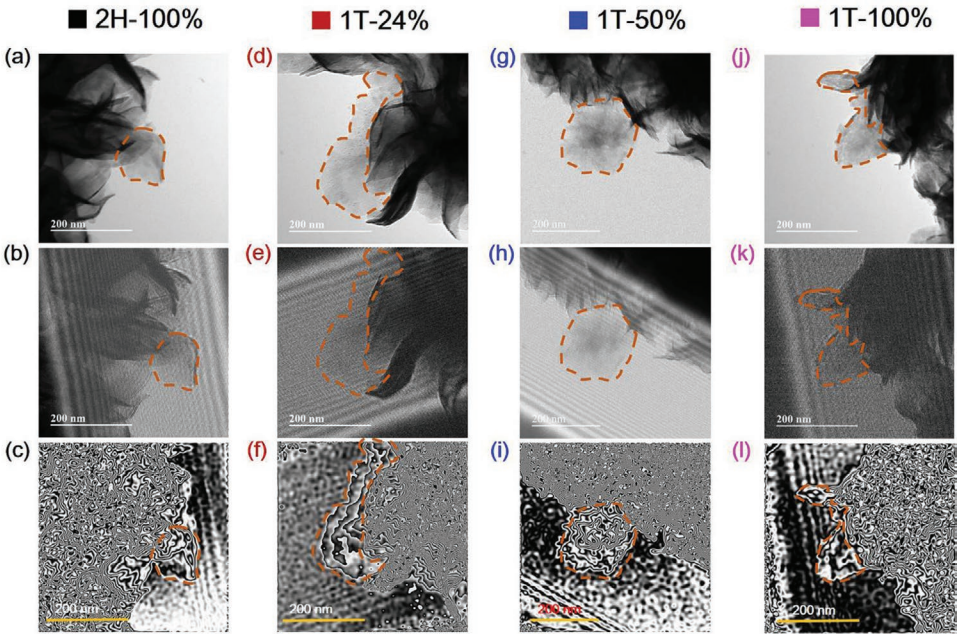

Figure 7. a,d,g,j) TEM images and (b,c,e,f,h,i,k,l) off-axis electron holograms of 2H-100% (a–c), 1T-24% (d–f), 1T-50% (g–i), and 1T-100% absorbers (j–l).

This could be confirmed by the EPR results as the 1T-50 wt% absorber shows the strongest EPR resonance (Figure 2i); and 3) the moderate enhanced conductivity alleviates the skin effect to exhibit the proper conductive loss during the incident EMW inside the absorbers (Figure 8a,b-iii). The conductive loss shows the upward trend as the increasing of metallic 1T phase in MoS_2. However, it should be noted that the high conductive values also lead to the deteriorative impedance and the following EMW absorbing performance (Figure 5d and Figure. 6d). In addition, the interlinked MoS_2 nanosheets also ensure the enlarged surface area for consuming the incident EMW effectively (i.e., the multiple scattering effect).

3. Conclusion

In summary, the dual-phase MoS_2 with linear 2H/1T phase ratio (with 0, 24, 50, and 100 wt% 1T) were synthesized by a magneto–hydrothermal method and the phase-dependent electromagnetic wave absorbing performance were systematically studied. The coexistence of 1T/2H multiphases in a single MoS_2 sheet optimized the inhomogeneous charge distribution and facilitated the electron behaviors, which boosted the EMW attenuation ability of absorbers. In particular, the 1T-50% MoS_2 absorber has been shown to be a satisfactory EMW absorber with an RL_{max} of –45.5 GHz and EAB of ≈3.89 dB. By using the

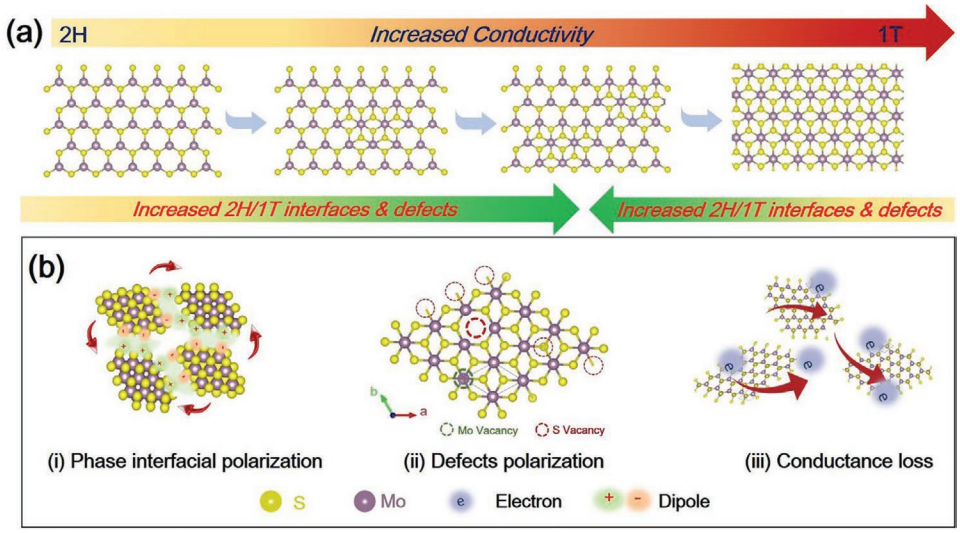

Figure 8. a) Phase-dependent conductivity, 2H/1T interfaces and defects of four MoS_2; b) phase interfacial i) and ii) defects polarization; iii) conductive loss mechanisms of four MoS_2 absorbers.

Lorentz TEM and CST simulation characterization, the 1T-50% absorber has been demonstrated to endow abundant interfaces between 2H and 1T phases, leading to the optimization of input impedance characteristics and boosted EMW absorbing ability. Taken together, the findings in the present work shed new light on the key roles played by manipulating the phase compositions and demonstrate a new pathway for optimization the EMW absorbing performance of TMDs absorbers.

4. Experimental Section

Preparation of 2D MoS_2: The 2D MoS_2 with different phase composition were synthesized based on our previous study.[15] In details, 1.4209 g thiourea and 0.7242 g $(NH_4)_6Mo_7O_{24}{\cdot}4H_2O$ were dissolved in deionized water (21.8 mL) and stirred for 1 h to get a homogeneous solution. After the mixture was transferred to Teflon-lined stainless-steel autoclave, a magnetic field was applied. The autoclave was sealed and heated to 210 °C in 40 min and kept for 18 h under different magnetic fields. Afterward, the autoclaves were naturally cooled to ambient temperature and the magnetic field was removed. Finally, the resulting product was filtered, washed several times by deionized water and ethanol, and dried under 70 °C overnight. According to the intensity of applied magnetic field (0T, 5T, and 9T), the products synthesized as above were denoted as MoS_2-0T, MoS_2-5T, and MoS_2-9T, respectively. The pure 2H-MoS_2 absorber were obtained by annealing the MoS_2-0T at 300 °C for 3 h with a ramping rate of 5 °C min^{-1}.

Preparation of 2D MoS_2/Wax: Specific quantities of 2D MoS_2 (40, 50, and 60 wt%) and paraffin (60, 50, and 40 wt%) were added to a vial containing an appropriate amount of ether and then treated ultrasonically for 1 h. The mixtures were cooled to room temperature and were pressed into a test sample (outer radius: 7.00 mm; inner radius: 3.04 mm) for dielectric measurement by coaxial method over 2–18 GHz as described in a previous work.[2b,5]

Characterizations: Powder XRD patterns were collected on a Bruker-AXS diffractometer (*Cu-K_α*). SEM and TEM images were obtained using FE-SEM-S-4800 and JEOL-2011 TEM. HAADF–STEM images were collected on a JEOL JEMARM200F at an acceleration voltage of 80 kV. Raman spectroscopy measurements were performed on a Lab RAM Aramis. XPS was carried out on a Kratos AXIS ULTRADLD (the power is 96 W and the pass energy of the XPS analyzer was set at 20 eV). Four-point probe (Keithley 4200-SCS) measurements were used to measure the electrical conductivity. The EPR spectra were performed with Bruker EMX Plus at room temperature operating at a frequency of ≈9.8 GHz. Field frequency modulation and microwave power were set to 100 kHz and 20 mW. The electro-holographies were carried out on a tailor-made Lorentz transmission electron microscope (JEM-2100F).

Electromagnetic Measurements: The relative permittivities (ε_r) and permeabilities (μ_r) of absorbers were measured on Agilent N5234A vector network analyzer over 2–18 GHz. The reflection losses (*RLs*) of absorbers were performed by using the transmission line Equation (1) and (2) as follows,[2b,c,8,13,28]

$$Z_{in} = Z_0 \cdot \sqrt{(\mu_r/\varepsilon_r)} \cdot \tanh\left[j \cdot (2\pi f d/c) \cdot \sqrt{\mu_r \varepsilon_r} \right] \quad (1)$$

$$RL = 20 \cdot \log\left|(Z_{in} - Z_0)/(Z_{in} + Z_0)\right| \quad (2)$$

In the formula, Z_0 is the impedance of air, Z_{in} the input impedance of the absorber, c the light velocity, f the electromagnetic wave frequency, and d the thickness of the absorber.

Attenuation Constant and Impedance Match Degree Calculation: The attenuation constant (α) and impedance match degree (Δ) were calculated according to the formulas as follows,[1a,9b,26,29]

$$a = \frac{\sqrt{2}\pi f}{c}\sqrt{(\mu''\varepsilon'' - \mu'\varepsilon') + \sqrt{(\mu''\varepsilon'' - \mu'\varepsilon')^2 + (\mu'\varepsilon'' + \mu''\varepsilon')^2}} \quad (3)$$

$$\Delta = \left|\sinh^2(Kfd) - M\right| \quad (4)$$

in which the f is the microwave frequency, d is the thickness of the absorber, c is the velocity of light, and K, M values were obtained according to the detailed equations as described in Figure S11, Supporting Information.

CST Simulations: The electric field distribution was performed using the finite integration technique on the Computer Simulation Technology (CST) Microware Studio 2014 package. According to the intrinsic 2D status of MoS_2, the CST simulation model was constructed by stacking ten MoS_2 laminations (0.3 mm per layer), in which the unit cell boundary conditions were applied in *X*/*Y* axis and the EMW was generated along −*Z* direction as demonstrated in Figure S12, Supporting Information.

Supporting Information

Supporting Information is available from the Wiley Online Library or from the author.

Acknowledgements

M.Q.N. acknowledges support from postdoc startup funding by the Ningbo Institute of Materials Technology & Engineering, CAS. The authors gratefully acknowledge the financial support by the National Key R&D Program of China (2016YFE0126700), National Natural Science Foundation of China (51525103, 51972029, and 11904116), and Technology Major Project of Ningbo (2018B10085).

Conflict of Interest

The authors declare no conflict of interest.

Data Availability Statement

The data that support the findings of this study are available from the corresponding author upon reasonable request.

Keywords

CST simulation, Lorentz TEM, microwave absorption, MoS_2, phase engineering

Received: December 30, 2020
Revised: January 26, 2021
Published online:

[1] a) X. Liang, X. Zhang, W. Liu, D. Tang, B. Zhang, G. Ji, *J. Mater. Chem. C* **2016**, *4*, 6816; b) M. Ning, B. Kuang, Z. Hou, L. Wang, J. Li, Y. Zhao, H. Jin, *Appl. Surf. Sci.* **2019**, *470*, 899; c) P. Wang, G. Wang, J. Zhang, B. Duan, L. Zheng, S. Zhang, D. He, T. Wang, *Chem. Eng. J.* **2020**, *382*, 122804; d) X. Zeng, X. Cheng, R. Yu, G. D. Stucky, *Carbon* **2020**, *168*, 606; e) H. Lv, Z. Yang, P. L. Wang, G. Ji, J. Song, L. Zheng, H. Zeng, Z. J. Xu, *Adv. Mater.* **2018**, *30*, 1706343; f) X. X. Wang, W. Q. Cao, M. S. Cao, J. Yuan, *Adv. Mater.* **2020**, *32*, 2002112.

[2] a) L. Cui, C. Tian, L. Tang, X. Han, Y. Wang, D. Liu, P. Xu, C. Li, Y. Du, *ACS Appl. Mater. Interfaces* **2019**, *11*, 31182; b) M. Ning,

Q. Man, G. Tan, Z. Lei, J. Li, R. W. Li, *ACS Appl. Mater. Interfaces* **2020**, *12*, 20785; c) X. Li, X. Yin, C. Song, M. Han, H. Xu, W. Duan, L. Cheng, L. Zhang, *Adv. Funct. Mater.* **2018**, *28*, 1803938.

[3] a) F. Tao, M. Green, A. T. V. Tran, Y. Zhang, Y. Yin, X. Chen, *ACS Appl. Nano Mater.* **2019**, *2*, 3836; b) X. Zhang, J. Xu, H. Yuan, S. Zhang, Q. Ouyang, C. Zhu, X. Zhang, Y. Chen, *ACS Appl. Mater. Interfaces* **2019**, *11*, 39100.

[4] a) W. Choi, N. Choudhary, G. H. Han, J. Park, D. Akinwande, Y. H. Lee, *Mater. Today* **2017**, *20*, 116; b) S. Manzeli, D. Ovchinnikov, D. Pasquier, O. V. Yazyev, A. Kis, *Nat. Rev. Mater.* **2017**, *2*, 17033; c) Y. Feng, T. Zhang, J. Zhang, H. Fan, C. He, J. Song, *Small* **2020**, *16*, 2002850.

[5] M. Q. Ning, M. M. Lu, J. B. Li, Z. Chen, Y. K. Dou, C. Z. Wang, F. Rehman, M. S. Cao, H. B. Jin, *Nanoscale* **2015**, *7*, 15734.

[6] D. Zhang, T. Liu, J. Cheng, Q. Cao, G. Zheng, S. Liang, H. Wang, M.-S. Cao, *Nano-Micro Lett.* **2019**, *11*, 38.

[7] D. Zhang, H. Zhang, J. Cheng, H. Raza, T. Liu, B. Liu, X. Ba, G. Zheng, G. Chen, M. Cao, *J. Mater. Chem. C* **2020**, *8*, 5923.

[8] Y. Sun, W. Zhong, Y. Wang, X. Xu, T. Wang, L. Wu, Y. Du, *ACS Appl. Mater. Interfaces* **2017**, *9*, 34243.

[9] a) X. Ding, Y. Huang, S. Li, N. Zhang, J. Wang, *Composites, Part A* **2016**, *90*, 424. b) H. Guo, L. Wang, W. You, L. Yang, X. Li, G. Chen, Z. Wu, X. Qian, M. Wang, R. Che, *ACS Appl. Mater. Interfaces* **2020**, *12*, 16831.

[10] a) W. Zhang, X. Zhang, Y. Zheng, C. Guo, M. Yang, Z. Li, H. Wu, H. Qiu, H. Yan, S. Qi, *ACS Appl. Nano Mater.* **2018**, *1*, 5865; b) J. Liu, H. Liang, H. Wu, *Composites, Part A* **2020**, *130*, 105760.

[11] a) A. Kuc, T. Heine, *Chem. Soc. Rev.* **2015**, *44*, 2603; b) W. Ye, F. Wu, N. Shi, H. Zhou, Q. Chi, W. Chen, S. Du, P. Gao, H. Li, S. Xiong, *Small* **2020**, *16*, 1906607; c) K. Leng, Z. Chen, X. Zhao, W. Tang, B. Tian, C. T. Nai, W. Zhou, K. P. Loh, *ACS Nano* **2016**, *10*, 9208; d) Y. Shao, J. H. Fu, Z. Cao, K. Song, R. Sun, Y. Wan, A. Shamim, L. Cavallo, Y. Han, R. B. Kaner, V. C. Tung, *ACS Nano* **2020**, *14*, 7308; e) S. Shi, Z. Sun, Y. H. Hu, *J. Mater. Chem. A* **2018**, *6*, 23932; f) K. A. Duerloo, Y. Li, E. J. Reed, *Nat. Commun.* **2014**, *5*, 4214.

[12] G. Eda, H. Yamaguchi, D. Voiry, T. Fujita, M. Chen, M. Chhowalla, *Nano Lett.* **2011**, *11*, 5111.

[13] W. Ding, L. Hu, Q. C. Liu, Z. G. Sheng, J. M. Dai, X. B. Zhu, Y. P. Sun, *Appl. Phys. Lett.* **2018**, *113*, 243102.

[14] F. Wypych, R. Schöllhorn, *J. Chem. Soc., Chem. Commun.* **1992**, 1386.

[15] W. Ding, L. Hu, J. Dai, X. Tang, R. Wei, Z. Sheng, C. Liang, D. Shao, W. Song, Q. Liu, M. Chen, X. Zhu, S. Chou, X. Zhu, Q. Chen, Y. Sun, S. X. Dou, *ACS Nano* **2019**, *13*, 1694.

[16] a) Z. Lei, J. Zhan, L. Tang, Y. Zhang, Y. Wang, *Adv. Energy Mater.* **2018**, *8*, 1703482; b) S. Jayabal, J. Wu, J. Chen, D. Geng, X. Meng, *Mater. Today Energy* **2018**, *10*, 264; c) L. Cai, J. He, Q. Liu, T. Yao, L. Chen, W. Yan, F. Hu, Y. Jiang, Y. Zhao, T. Hu, Z. Sun, S. Wei, *J. Am. Chem. Soc.* **2015**, *137*, 2622.

[17] P. de Rango, M. Lees, P. Lejay, A. Sulpice, R. Tournier, M. Ingold, P. Germi, M. Pernet, *Nature* **1991**, *349*, 770.

[18] a) W. Zhang, X. Liao, X. Pan, M. Yan, Y. Li, X. Tian, Y. Zhao, L. Xu, L. Mai, *Small* **2019**, *15*, 1900964; b) Q. Liu, X. Li, Q. He, A. Khalil, D. Liu, T. Xiang, X. Wu, L. Song, *Small* **2015**, *11*, 5556.

[19] a) L. Cheng, Y. Liu, *J. Am. Chem. Soc.* **2018**, *140*, 17895; b) M. Acerce, D. Voiry, M. Chhowalla, *Nat. Nanotechnol.* **2015**, *10*, 313.

[20] X.-J. Zhang, S. Li, S.-W. Wang, Z.-J. Yin, J.-Q. Zhu, A.-P. Guo, G.-S. Wang, P.-G. Yin, L. Guo, *J. Phys. Chem. C* **2016**, *120*, 22019.

[21] X. Wang, W. Ding, H. Li, H. Li, S. Zhu, X. Zhu, J. Dai, Z. Sheng, H. Wang, X. Zhu, Y. Sun, S. X. Dou, *J. Mater. Chem. A* **2019**, *7*, 19152.

[22] Q. Ke, X. Zhang, W. Zang, A. M. Elshahawy, Y. Hu, Q. He, S. J. Pennycook, Y. Cai, J. Wang, *Small* **2019**, *15*, e1900131.

[23] J. Wang, Y. Cui, F. Wu, T. Shah, M. Ahmad, A. Zhang, Q. Zhang, B. Zhang, *Carbon* **2020**, *165*, 275.

[24] L. Liang, R. Yang, G. Han, Y. Feng, B. Zhao, R. Zhang, Y. Wang, C. Liu, *ACS Appl. Mater. Interfaces* **2020**, *12*, 2644.

[25] M. M. Lu, W. Q. Cao, H. L. Shi, X. Y. Fang, J. Yang, Z. L. Hou, H.-B. Jin, W. Z. Wang, J. Yuan, M. S. Cao, *J. Mater. Chem. A* **2014**, *2*, 10540.

[26] X. Jian, W. Tian, J. Li, L. Deng, Z. Zhou, L. Zhang, H. Lu, L. Yin, N. Mahmood, *ACS Appl. Mater. Interfaces* **2019**, *11*, 15869.

[27] Z. Wu, K. Pei, L. Xing, X. Yu, W. You, R. Che, *Adv. Funct. Mater.* **2019**, *29*, 1901448.

[28] Y. Li, X. Liu, X. Nie, W. Yang, Y. Wang, R. Yu, J. Shui, *Adv. Funct. Mater.* **2019**, *29*, 1807624.

[29] D. Zhang, Y. Xiong, J. Cheng, J. Chai, T. Liu, X. Ba, S. Ullah, G. Zheng, M. Yan, M. Cao, *Sci. Bull.* **2020**, *65*, 138.